8

Research Article

Anwar Ali Aldhafeeri* and Humaira Yasmin*

A numerical analysis of the rotational flow of a hybrid nanofluid past a unidirectional extending surface with velocity and thermal slip conditions

https://doi.org/10.1515/rams-2024-0052 received March 02, 2024; accepted July 07, 2024

Abstract: This work inspects 3D magnetohydrodynamic hybrid nanofluid flow on a permeable elongating surface. The emphasis of this paper is on the study of hybrid nanofluid flow within a rotating frame, taking into account the simultaneous impact of both thermal and velocity slip boundary conditions. The chosen base fluid is water, and the hybrid nanofluid comprises two nanoparticles Cu and Al₂O₃. The effect of the magnetic and porosity parameters is taken into account in the momentum equation. The thermal radiation, Joule heating, and heat source are considered in the energy equation. Using a similarity system, we transform the PDEs of the proposed model into ODEs, which are then solved numerically by the bvp4c technique. The magnetic field shows a dual nature on primary and secondary velocities. Enrich magnetic field decreases the primary velocity and enhances the secondary velocity. The rotation parameter has an inverse relation with both velocities. The temperature profile amplified with the escalation in heat source, magnetic field, rotation factor, and Eckert numbers. The skin friction is boosted with magnetic parameters while the Nusselt number drops.

Keywords: nanofluid, hybrid nanofluid, MHD, porous medium, viscous dissipation, Joule heating, rotational flow

Nomenclature

$K_{ m p}$	porosity parameter
u, v, w	velocity along x -, y - and z - axis
x, y, z	coordinates of axis
Ec	Eckert number
M	magnetic parameter
$Q_{\rm t}$	heat generation parameter
Ω	angular velocity
γ_1	velocity slip parameter
γ_2	thermal slip parameter
а	constant number
μ	dynamic viscosity
k	thermal conductivity
B_0	strength of the magnetic field
T , T_{∞}	fluid and ambient temperatures
Pr	Prandtl number
Sk_x	skin friction coefficient
C , C_{∞}	fluid and ambient concentrations
Nu_n	Nusselt number
Re	Reynolds number
$(C_{\rm p})$	specific heat
Sc	Schmidt number
σ	electrical conductivity
C_{w}	surface concentration
Rd	thermal radiation
σ^*	Stefan–Boltzmann constant
ho	density
f	base fluid

1 Introduction

nanofluid hybrid nanofluid

Nanofluid is a colloidal suspension comprising nanometersized solid particles, typically metal or oxide nanoparticles, dispersed within a base fluid. These engineered fluids exhibit unique thermophysical features, including enhanced thermal

nf

hnf

^{*} Corresponding author: Anwar Ali Aldhafeeri, Department of Mathematics and Statistics, Faculty of Science, King Faisal University, P.O. Box 400, Al Ahsa, 31982, Saudi Arabia, e-mail: aaaldhafeeri@kfu.edu.sa

^{*} Corresponding author: Humaira Yasmin, Department of Mathematics and Statistics, Faculty of Science, King Faisal University, P.O. Box 400, Al Ahsa, 31982, Saudi Arabia; Department of Basic Sciences, General Administration of Preparatory Year, King Faisal University, P.O. Box 400, Al Ahsa, 31982, Saudi Arabia, e-mail: hhassain@kfu.edu.sa

conductivity and heat transfer efficiency as first introduced by Choi [1]. The preparation involves scattering nanoparticles in a base fluid through two-step or one-step methods [2]. The effect of nanofluid flow on heat transfer is significant, primarily due to the engineered enhancement of thermophysical properties caused by mixing nanoparticles with pure fluid [3,4]. This heightened heat transfer efficiency is especially crucial in applications like coolant purposes for heat exchangers and electronic devices, etc. [5]. The increased heat-carrying capacity and improved thermal properties of nanofluids contribute to more efficient energy exchange and thermal management, making them highly desirable for escalating thermal transference in a variety of industrial processes and technological applications. Khan et al. [6] mixed nanoparticles of gold in blood to improve the thermal flow features of the resultant nanofluid and noticed that an upsurge in volume fractions of nanoparticles and permeability factor has declined in velocity characteristics and escalated the thermal distribution. Hybrid nanofluid flow involves the incorporation of multiple types of nanoparticles or a combination of nanoparticles with other additives in a base fluid [7]. The purpose is to exploit synergistic effects and enhance specific properties tailored to the desired application. The impression of hybrid nanofluid flow on thermal transference is multifaceted. By combining different nanoparticles, researchers aim to achieve optimized thermophysical features and improved stability of pure fluids [8]. Additionally, hybrid nanofluids offer the flexibility to tailor the fluid's properties to suit diverse applications, ranging from electronics cooling to industrial heat exchangers [9]. Ali et al. [10] investigated computationally trihybrid nanofluid flow with thermal slip effects on an elongating sheet. Nagaraja et al. [11] examined mass and thermal transportations to assess opposing radiative trihybrid nanofluid flow on exponentially elongating surfaces. By adding nonlinear thermal radiation over the exponentially extensible surface, Darvesh et al. [12] investigated the global warming effect using magnetohydrodynamic (MHD) nanofluid. Their research led them to the conclusion that increased radiation is amplifying the effects of both global warming and solar power. Using the cross model's infinite shear rate viscosity, Tag EI Din et al. [13] investigated the energy melting process impacted by the cross nanofluid's inclined magnetic field across the wedge's geometry. The researchers discovered that as the magnetic and viscosity parameters increase, the velocity profile becomes more distinct. The behavior of the stagnation point flow of Carreau nanofluid that was attached to a slanted magnetic effect was studied by EI Din et al. [14]. In order to obtain the numerical result, they utilized the spectrum relaxation approach. The quadratic multiple regression model was utilized in order to ascertain

the rate of heat transition concerning the Nusselt number during the process.

MHD is a field of science that studies the dynamics of electrically conductive fluids under the impact of magnetic fields [15]. The collaboration between magnetic fields and fluid dynamics introduces compelling effects on convective heat transfer, particularly in scenarios involving plasmas, liquid metals, and electrolytes [16]. The Lorentz force, a product of the interaction between magnetic fields and electric currents within the fluid, plays a pivotal role in inducing fluid motion. This force alters the velocity distribution, impacting convective heat transfer rates, MHD has notable applications in nuclear power systems, where it is employed to optimize heat transfer and enhance system efficiency [17]. Safdar et al. [18] determined solutions in analytical form for MHD fluid flow for time-dependent thin film on a stretching surface. Challenges associated with MHD-induced heat transfer include increased pressure drop, potential fluid instabilities, and the complex relationship between magnetic fields and fluid flow. Researchers employ numerical simulations and experimental studies to elucidate these phenomena, utilizing computational models rooted in MHD equations [19]. As emerging technologies, such as MHD pumps and generators, continue to develop, MHD's impact on heat transfer in fluid flow becomes increasingly crucial, with implications for space exploration, advanced power generation, and other innovative applications requiring efficient thermal management in electrically conductive fluids subjected to magnetic fields [20,21]. Understanding and harnessing these MHD effects are fundamental for advancing heat transfer processes across various industrial and scientific domains. An investigation was carried out [22] using numerical methods to determine the infinite shear rate of Carreau nanofluid with an inclined magnetic dipole over a cylindrical channel. In their investigation, they found that the velocity curve was lowered by both magnetic and infinite shear rates.

A porous medium refers to a substance or structure that contains interrelated void spaces, allowing the flow of fluids through such a surface. These void spaces can be filled with a gas, liquid, or a combination of both. Porous media are encountered in various natural and engineered systems, including soils, rocks, foams, and certain types of materials with complex internal structures [23,24]. The presence of pores in a permeable medium significantly influences fluid flow and thermal transference. In the context of heat transfer for fluid flow, the porous structure alters the convective heat transfer process [25]. The complex network of pores creates additional pathways for the fluid to flow, enhancing convective heat transfer coefficients. This increased convective heat transfer is particularly relevant in applications

such as geothermal systems, underground heat exchangers, and catalytic converters, where porous media contribute to improved thermal performance and energy efficiency [26,27]. The porous medium's impact on fluid flow and heat transfer is crucial for optimizing processes in numerous fields, ranging from environmental engineering to industrial applications. Researchers employ mathematical models, numerical simulations, and experimental studies to explore and quantify the heat transfer characteristics within porous media, advancing our comprehension of these complex phenomena and facilitating the design of more efficient thermal systems. A numerical approach was investigated by Darvesh et al. [28] with relation to a variable viscosity-based mixed convective inclined magnetized cross nanofluid that was applied to a spongy surface with varied thermal conductivities. As a result of their investigation, they discovered that the Brownian motion parameter velocity decreased as the suction increased. Rakpakdee et al. [29] examined heat transportation features for the MHD flow of fluid on a permeable media and proved that the velocity panels weakened while thermal panels augmented with escalation magnetic and porosity factors. An investigation on the stagnation point flow over a porous extended surface with slip condition was carried out by Ayub et al. [30]. The spectrum relaxation strategy, which is based on the Gauss-Seidel relaxation method is also utilized in order to solve the ordinary differential equations. Based on the numerical result, it is found that a significant change in the Nusselt number was discovered with the growing values of the thermophoresis factor.

Joule heating is a process in which heat is produced within a conductor or resistive material as a result of the passage of electric current through it [31]. Joule first experimentally demonstrated the relationship between electrical current and heat generation, Joule heating arises for confrontation faced by the electric current as it passes in a conductor, according to Joule's law. The process involves the exchange of electrical energy into thermal energy within the material, leading to a temperature increase [32]. The impacts of Joule heating on thermal transportation are profound, influencing various technological applications. In electrical systems and devices, such as resistive heating elements and electrical circuits, Joule heating is a crucial consideration as it determines the amount of heat generated during the flow of current [33]. While Joule heating is often an undesirable effect due to potential energy losses and heat dissipation in electronic components, it is also harnessed intentionally in devices such as electric heaters, toasters, and incandescent light bulbs, where the generated heat is the desired outcome. In the field of microelectronics, managing and dissipating Joule heat is critical for preventing overheating and ensuring the

reliability of electronic devices [34]. Additionally, Joule heating plays a role in various industrial processes, including welding and material processing, where the controlled application of electrical current induces localized heating for specific purposes. Mitigating the effects of Joule heating is essential for optimizing the effectiveness of electronic and thermal systems, influencing the design and development of technologies that rely on the controlled generation and dissipation of heat through electrical currents. Similar concepts can be studied in refs. [35-39].

Rotational flow, also known as swirling or vortex flow, is a fluid motion pattern characterized by the rotation of fluid elements around an axis [40]. This sort of flow is generally perceived in scenarios where angular momentum is imparted to the fluid, leading to a rotational or swirling motion. The impacts of rotational flow on thermal transportation and velocity distribution are significant, especially in applications such as rotating machinery, heat exchangers, and cyclonic separators [41]. This is particularly advantageous in heat exchangers, where improved thermal transportation efficiency is crucial. The velocity distribution in rotational flow exhibits variations compared to straight or laminar flows [42]. Near the axis of rotation, velocities tend to be higher, creating a central core of faster-moving fluid, while the outer regions experience lower velocities. This velocity profile influences the heat transfer characteristics, as regions with higher velocities typically exhibit enhanced convective heat transfer. Velocity and thermal effects are essential in the scheme and system's optimization involving rotational flow, allowing engineers to tailor fluid dynamics for improved heat transfer performance [43]. Khan et al. [44] inspected rotary motion for MHD fluid flow on a spinning cylinder and used dissipative effects on fluid flow. Furthermore, the impacts of rotational flow on thermal transportation extend to environmental fluid dynamics, where phenomena like atmospheric vortices and oceanic gyres play a crucial role in heat and energy distribution within the Earth's atmosphere and oceans [45]. Kumar et al. [46] discussed nanofluid flow with rotational effects on a gyrating sphere using heat absorption and generation.

In the light of above literature, the MHD three-dimensional hybrid nanofluid flows through a spongy extending surface with velocity and thermal boundary conditions in a porous medium. Two different kinds of nanoparticles, i.e., copper and alumina, are mixed into water to produce a hybrid nanofluid. In the current model, velocity and thermal slip constraints are used. The equations that are responsible for the flow are transformed into nonlinear ODEs via the selfsimilar method. A numerical approach called bvp4c is utilized for the solution of resultant equations. The impacts of several physical factors in the presence and absence of velocity and thermal slip constraints are discussed through graphs and Tables.

2 Mathematical model

Take 3D hybrid nanofluid flow on a permeable extending sheet is examined. Assume that the fluid is viscous and incompressible. The coordinates of the flow are x, y and zalong with velocities u, v and w respectively. The fluid moves in the x- direction with velocity $u = u_w(=ax)$ as illustrated in Figure 1. The fluid is rotating about the z- axis with angular velocity Ω_1 . The surface temperature and concentration are T_w and C_w while at infinity, their corresponding notations are T_{∞} and C_{∞} . A transversal magnetic field with B_0 as its strength is applied along z- axis, i.e., perpendicular to both x- and y- axis. The Joule heating, heat source, and thermal radiation are considered in the heat equation. Additionally, supposed that the induced magnetic field is lesser in comparison to the external magnetic field. Furthermore, velocity and thermal slip constraints are considered at the surface [47,48]. By implementing the proposed conditions, we obtain

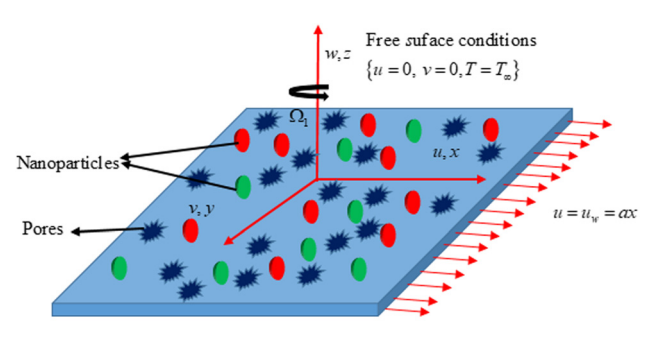
$$\frac{\partial u}{\partial x} + \frac{\partial v}{\partial y} + \frac{\partial w}{\partial z} = 0, \tag{1}$$

$$\rho_{\rm hnf} \left[u \frac{\partial u}{\partial x} + v \frac{\partial u}{\partial y} + w \frac{\partial u}{\partial z} - 2\Omega_1 v \right]$$

$$= \mu_{\rm hnf} \frac{\partial^2 u}{\partial z^2} - \sigma_{\rm hnf} B_0^2 u - \frac{\mu_{\rm hnf}}{k_{\rm p}} u,$$
(2)

$$\rho_{\rm hnf} \left[u \frac{\partial v}{\partial x} + v \frac{\partial v}{\partial y} + w \frac{\partial v}{\partial z} + 2\Omega_1 u \right]$$

$$= \mu_{\rm hnf} \frac{\partial^2 v}{\partial z^2} - \sigma_{\rm hnf} B_0^2 v - \frac{\mu_{\rm hnf}}{k_{\rm p}} v,$$
(3)



$$\left\{ u = u_{w}\left(x\right) + S_{1} \frac{\partial u}{\partial z}, v = 0, w = 0, T = T_{w} + S_{2} \frac{\partial T}{\partial z} \right\}$$
Surface conditions

Figure 1: Geometry of the flow problem.

$$(\rho C_{\rm P})_{\rm hnf} \left[u \frac{\partial T}{\partial x} + v \frac{\partial T}{\partial y} + w \frac{\partial T}{\partial z} \right]$$

$$= k_{\rm hnf} \frac{\partial^2 T}{\partial z^2} - \frac{\partial q_a}{\partial z} + \sigma_{\rm hnf} B_0^2 (u^2 + v^2) + Q_0 (T - T_{\infty})$$

$$+ \mu_{\rm hnf} \left[\left(\frac{\partial u}{\partial z} \right)^2 + \left(\frac{\partial v}{\partial z} \right)^2 \right],$$
(4)

The boundary constraints are [49]

$$u = u_{\rm w}(x) + S_1 \frac{\partial u}{\partial z}, \quad v = 0, \quad w = 0, \quad T = T_{\rm w} + S_2 \frac{\partial T}{\partial z},$$

at $z \to 0$,
 $u \to 0, \quad v \to 0, \quad T \to T_{\infty}$ at $z \to \infty$. (5)

The similarity transformations are

$$u = axf'(\xi), \quad v = axg(\xi), \quad w = -\sqrt{a\vartheta_{\rm f}}(f(\xi)),$$

$$\theta(\xi) = \frac{T - T_{\infty}}{T_{\rm tr} - T_{\infty}}, \quad \xi = z\sqrt{\frac{a}{\vartheta_{\rm f}}}.$$
(6)

Here, S_1 and S_2 are the velocity and temperature slip, respectively. A radiative heat flux is taken into consideration, and this may be approximated by utilizing the Rosseland approximation, which is derived from the idea of diffusion. The radiative heat flux q_a along the z- direction is defined below [50]:

$$q_{\rm a} = -\frac{4\sigma^*}{3k^*} \frac{\partial T^4}{\partial z}.$$
 (7)

Taylor series for T^4 is given as

$$T^4 = 4T_{\infty}^3 T - 3T_{\infty}^3 (T - T_{\infty}) + 6T_{\infty}^2 (T - T_{\infty})^2 + \dots$$
 (8)

Neglect the higher order term, in above Eq. (8), beyond the 1st degree in $(T - T_{\infty})$, we obtain

$$T^4 = 4T_m^3 T - 3T_m^3. (9)$$

Putting Eqs. (8) and (9) in Eq. (7), the following result is obtained:

$$q_{\rm a} = -\frac{16\sigma^* T_{\infty}^3}{3k^*} \frac{\partial T}{\partial z}.$$
 (10)

Simplified forms of the equations via similarity transformations are

$$\frac{A_1}{A_2}f''' - f'^2 + ff'' + 2\Omega g - \frac{A_3}{A_2}Mf' - \frac{A_1}{A_2}K_pf' = 0, \quad (11)$$

$$\frac{A_1}{A_2}g'' - gf' + fg' - 2\Omega f' - \frac{A_3}{A_2}Mg - \frac{A_1}{A_2}K_pg = 0, \quad (12)$$

$$\frac{1}{A_5} \left[A_4 + \frac{4}{3} \text{Rd} \right] \theta'' + \text{Pr} f \theta' + \frac{1}{A_5} Q_t \theta
+ \frac{A_3}{A_5} M \text{EcPr} (f'^2 + g^2) + \frac{A_1}{A_5} \text{EcPr} (f''^2 + g'^2) = 0.$$
(13)

The subjected constraints at the boundary are

$$f'(0) = 1 + \gamma_1 f''(0), \ g(0) = 0,$$

$$\theta(0) = 1 + \gamma_2 \theta'(0), \ f(0) = 0,$$

$$f'(\infty) = 0, \ \theta(\infty) = 0, \ g(\infty) = 0.$$
(14)

$$\begin{split} &\Pr\!\left(=\frac{\vartheta_{\rm f}(\rho C_{\rm p})_{\rm f}}{k_{\rm f}}\right) \text{ is Prandtl number, } \gamma_1\!\!\left(=\!S_1\sqrt{\frac{a}{\vartheta_{\rm f}}}\right) \text{ is the velocity slip factor, } K_{\rm p}\!\!\left(=\!\frac{\mu_{\rm f}}{\rho_{\rm f}ak_{\rm p}}\right) \text{ is the porosity parameter, } \varOmega\!\!\left(=\!\frac{\varOmega_1}{a}\right) \\ &\text{is the rotation factor, } \mathrm{Rd}\!\!\left(=\!\frac{4\sigma^*T_\infty^3}{k^*k_{\rm f}}\right) \text{ is the radiation factor, } \\ &M\!\!\left(=\!\frac{\sigma_{\rm f}B_0^2}{\rho_{\rm f}a}\right) \quad \text{is the magnetic parameter, heat source} \\ &Q_{\rm t}\!\!\left(=\!\frac{Q_0}{a(\rho C_{\rm p})_{\rm f}}\right)\!\!, \text{ and Eckert number is Ec}\!\!\left(=\!\frac{u_{\rm w}^2}{(C_{\rm p})_{\rm f}(T_{\rm w}-T_\infty)}\right)\!\!. \\ &\text{Here, } \quad A_1=\frac{\mu_{\rm hnf}}{\mu_{\rm f}}, \quad A_3=\frac{\sigma_{\rm hnf}}{\sigma_{\rm f}}, \quad A_2=\frac{\rho_{\rm hnf}}{\rho_{\rm f}}, \quad A_4=\frac{k_{\rm hnf}}{k_{\rm f}}, \\ &\text{and } A_5=\frac{(\rho C_{\rm p})_{\rm hnf}}{(\rho C_{\rm p})_{\rm f}}. \end{split}$$

The thermophysical property of nanoparticles and base fluid are defined as follows:

$$\frac{\mu_{\text{hnf}}}{\mu_{\text{f}}} = \frac{1}{(1 - \phi_{1})^{2.5}(1 - \phi_{2})^{2.5}}$$

$$\frac{\rho_{\text{hnf}}}{\rho_{\text{f}}} = (1 - \phi_{2}) \left\{ 1 - \phi_{1} + \phi_{1} \frac{\rho_{1}}{\rho_{\text{f}}} \right\} + \phi_{2} \frac{\rho_{2}}{\rho_{\text{f}}}$$

$$\frac{(\rho C_{\text{p}})_{\text{hnf}}}{(\rho C_{\text{p}})_{\text{f}}} = (1 - \phi_{2}) \left\{ 1 - \phi_{1} + \phi_{1} \frac{(\rho C_{\text{p}})_{1}}{(\rho C_{\text{p}})_{\text{f}}} \right\} + \phi_{2} \frac{(\rho C_{\text{p}})_{2}}{(\rho C_{\text{p}})_{\text{f}}},$$

$$\frac{k_{\text{hnf}}}{k_{\text{f}}} = \frac{k_{2} + 2k_{\text{bf}} + 2\phi_{2}(k_{2} - k_{\text{f}})}{k_{2} + 2k_{\text{bf}} - \phi_{2}(k_{2} - k_{\text{f}})} \text{ where}$$

$$\frac{k_{\text{nf}}}{k_{\text{f}}} = \frac{k_{1} + 2k_{\text{f}} + 2\phi_{1}(k_{1} - k_{\text{f}})}{k_{1} + 2k_{\text{f}} - \phi_{1}(k_{1} - k_{\text{f}})}$$

$$\frac{\sigma_{\text{hnf}}}{\sigma_{\text{f}}} = \frac{\sigma_{2} + 2\sigma_{\text{bf}} + 2\phi_{2}(\sigma_{2} - \sigma_{\text{f}})}{\sigma_{2} + 2\sigma_{\text{bf}} - \phi_{2}(\sigma_{2} - \sigma_{\text{f}})}$$

$$\frac{\sigma_{\text{nf}}}{\sigma_{\text{f}}} = \frac{\sigma_{1} + 2\sigma_{\text{f}} + 2\phi_{1}(\sigma_{1} - \sigma_{\text{f}})}{\sigma_{1} + 2\sigma_{\text{f}} - \phi_{1}(\sigma_{1} - \sigma_{\text{f}})}.$$

Relevant physical quantities

The physical quantities, which are skin friction and Nusselt number, have great importance in engineering science and industrial process.

$$Cf_x = \frac{\tau_{wx}}{\rho_f u_w^2}$$
 and $Nu_s = \frac{xq_w}{k_f (T_w - T_\infty)}$. (16)

The shear stress $au_{\mathrm{W}\mathrm{X}}$ and surface heat flux q_{W} are demarcated as follows:

$$\begin{cases}
\tau_{wx} = \mu_{hnf} \frac{\partial u}{\partial z}, \\
q_{w} = -k_{hnf} \frac{\partial T}{\partial z} - q_{a}, \text{ at } z = 0
\end{cases}.$$
(17)

Using Eqs. (6) and (15) the simplified form of Eq. (14) is given by

$$\begin{cases} Sk_x = (Re_x)^{0.5} Cf_x = A_1 f''(0), \\ Nu_n = (Re_x)^{-0.5} Nu_s = -\left[A_4 + \frac{4}{3}Rd\right]\theta'(0) \end{cases}.$$
 (18)

4 Numerical procedure

Upon the transformation of flow field equations into ODEs, we utilize the byp4c technique in MATLAB designed for solving first-order ODEs. Consequently, we implement the following transformations to obtain the required equations.

$$L_{1} = f(\xi), \quad L_{2} = f'(\xi), \quad L_{3} = f''(\xi),$$

$$L'_{3} = f'''(\xi), \quad L_{4} = g(\xi),$$

$$L_{5} = g'(\xi), \quad L_{6} = g''(\xi), \quad L'_{6} = g'''(\xi),$$

$$L_{7} = \theta(\xi), \quad L_{8} = \theta'(\xi),$$

$$L'_{8} = \theta''(\xi),$$
(19)

Using Eq. (17), we write the equation from (9) to (12) in the following form:

$$L_{3}' = -\frac{A_{2}}{A_{1}} \left[L_{2}L_{2} + L_{1}L_{3} + 2\Omega L_{4} - \frac{A_{3}}{A_{2}}ML_{2} - \frac{A_{1}}{A_{2}}K_{p}L_{2} \right], (20)$$

$$L_{6}' = -\frac{A_{2}}{A_{1}} \left[-L_{4}L_{6} + L_{1}L_{5} - 2\Omega L_{2} - \frac{A_{3}}{A_{2}}ML_{4} - \frac{A_{1}}{A_{2}}K_{p}L_{4} \right], \quad (21)$$

$$L_8' = \frac{\Pr}{\left(A_4 + \frac{4}{3}\text{Rd}\right)} (A_5 L_1 L_8 + Qt L_7 + A_1 \text{Ec}(L_3 L_3 + L_5 L_5)$$

$$+ A_3 M \text{Ec}(L_2 L_2 + L_4 L_4)).$$
(22)

The new converted boundary circumstances are as follows:

Table 1: The thermophysical property of Cu and Al₂O₃ with H₂O [51]

Name	Base fluid	Nanoparticles	
	H_2O	Cu	Al_2O_3
ρ (kg · m ⁻¹)	997.1	8,933	3,970
$C_{\rm p} (J \cdot kg^{-1} \cdot k^{-1})$	4,179	385	765
$k (W \cdot m^{-1} \cdot k^{-1})$	0.613	400	40
σ (S·m ⁻¹)	5.5×10^{-6}	59.6 × 10 ⁶	35×10^{6}
Pr	6.2		

Table 2: Comparison of -f''(0) with different values of Ω

Ω	-f"(0)				
	Present work	Hussain et al. [52]	Nazir et al. [53]	Dawar et al. [48]	
0.0	1.000431	1.00426	1.0004310	1.000431	
0.5	1.172101	1.171890	1.171210	1.171210	
1.0	1.358190	1.353201	1.358181	1.358182	
2.0	1.681031	1.680331	1.681031	1.681031	

$$L_{2}(a) = 1 + \gamma_{1}L_{3}(a),$$

$$L_{1}(a) = 0, L_{2}(b) = 0,$$

$$L_{4}(a) = 0, L_{4}(b) = 0,$$

$$L_{7}(a) = 1 + \gamma_{2}L_{8}(a),$$

$$L_{7}(b) = 0.$$
(23)

5 Validation of code

Table 2 presents the validation of convergence criteria comparing -f''(0) with earlier published results. The finding in Table 2 indicates a noteworthy consistency between the present outcomes and the result reported by refs. [48,52,53] for several values of Ω discussed in their studies.

6 Discussion of results

Evaluating the set of ODEs, various numerical forms and their corresponding graphical outcomes are obtained. The focus of this paper is on the study of hybrid nanofluid flow

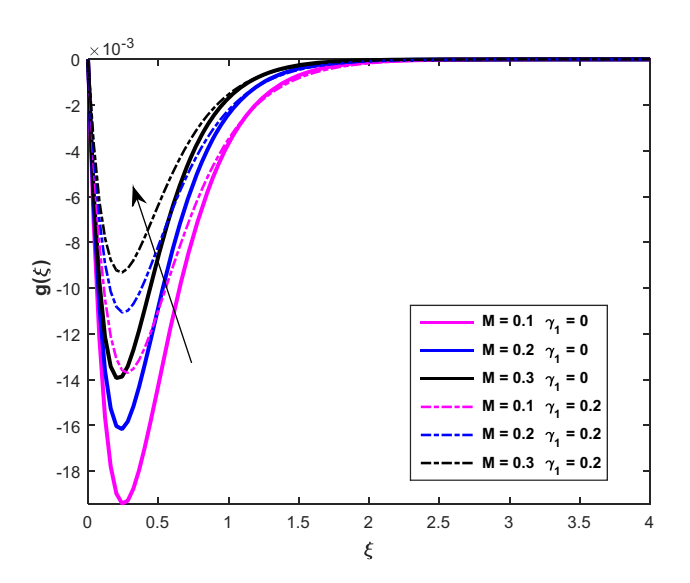


Figure 3: Fluctuation in $g(\xi)$ *via* M.

within a rotating frame taking into account the simultaneous impact of both thermal and velocity slip boundary conditions. These results are expressed in Figures 2–11 as well as in Tables 3 and 4. The effects of key factors are radiation (Rd), rotation (Ω), magnetic field (M) porosity (K_p), Eckert number (Ec), thermal slip (γ_2), velocity slip (γ_1) and heat source (Q_t) on primary velocity ($f'(\xi)$) secondary velocity ($g(\xi)$) and thermal field ($\theta(\xi)$). Eq. (15) represents the theoretical model of hybrid nanofluid. Incorporating fundamental factors like dynamic viscosity (μ) fluid density (ρ) heat capacitance (C_p) thermal conductivity (k) and electrical conductivity (σ) of the fluid. The subscripts (hnf), (nf) and (f) serve to differentiate between the hybrid, nanofluid and base fluid. Table 1 presents the

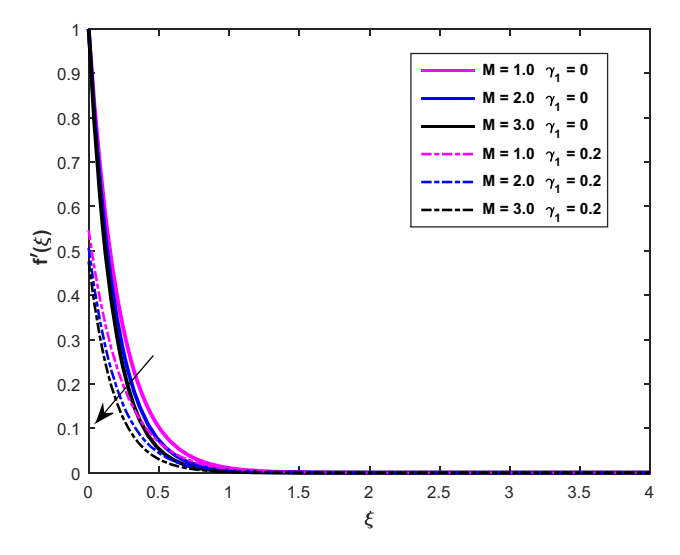


Figure 2: Fluctuation in $f'(\xi)$ *via* M.

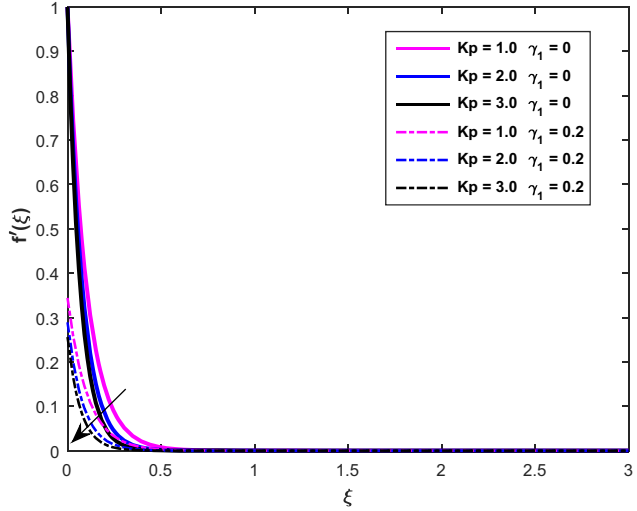


Figure 4: Fluctuation in $f'(\xi)$ via K_p .

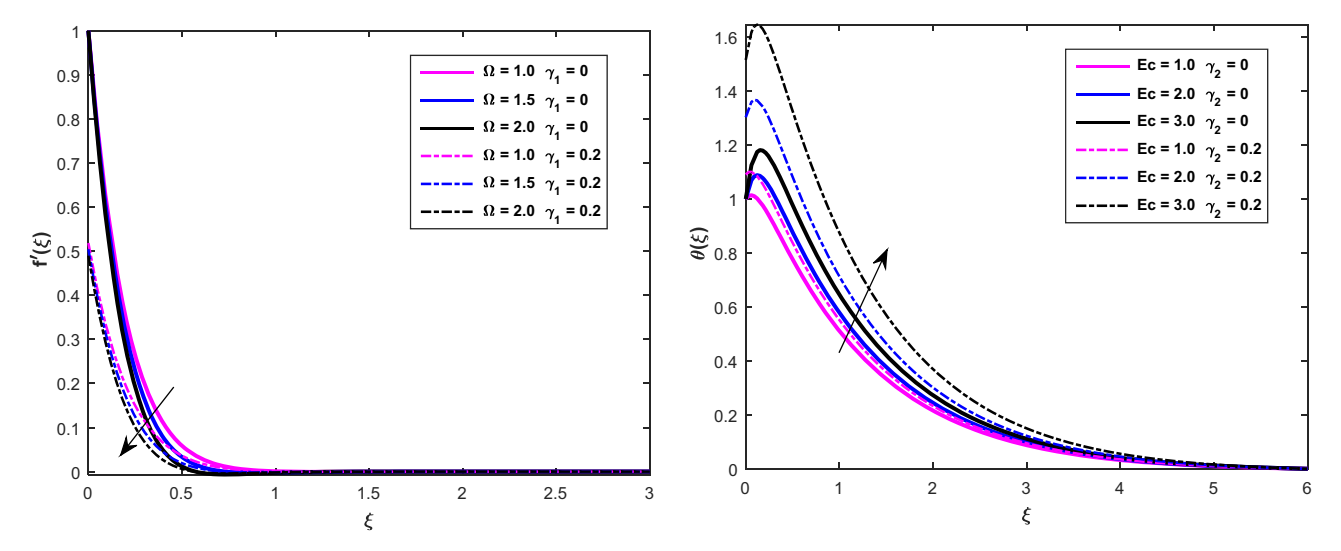


Figure 5: Fluctuation in $f'(\xi)$ via Ω .

Figure 8: Fluctuation in $\theta(\xi)$ *via* Ec.

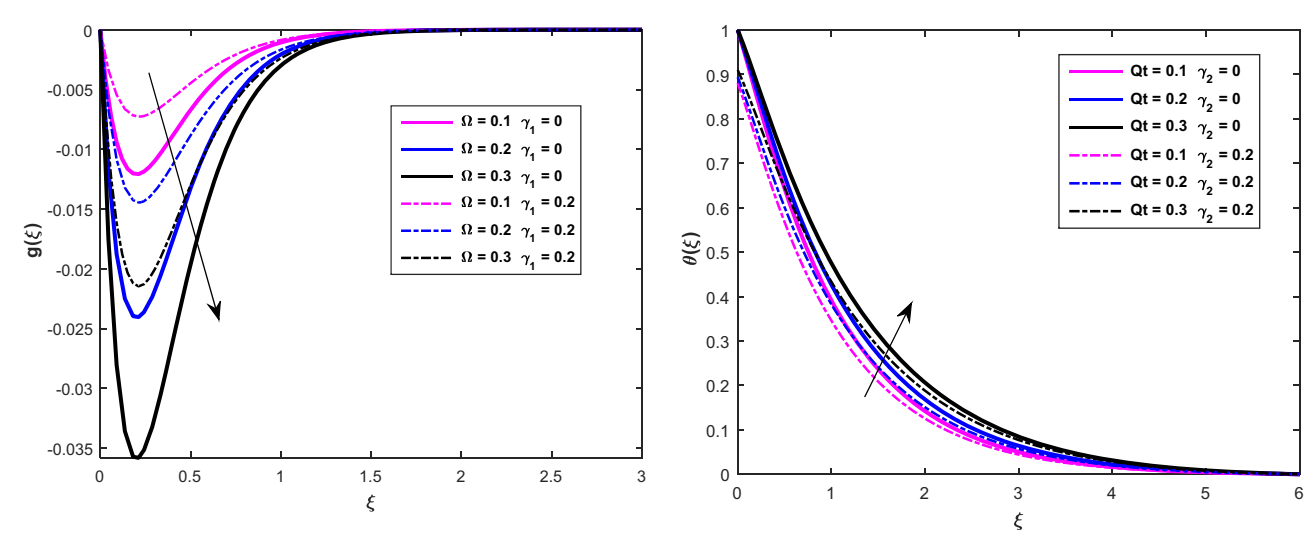


Figure 6: Fluctuation in $g(\xi)$ *via* Ω .

Figure 9: Fluctuation in $\theta(\xi)$ *via* Q_t .

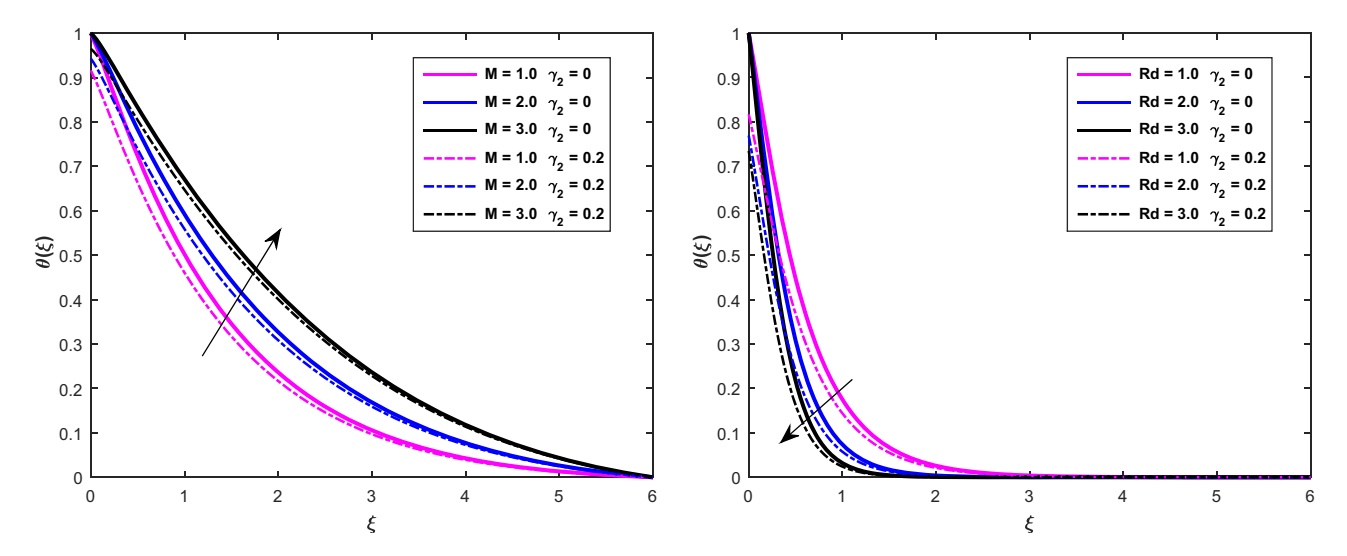


Figure 7: Fluctuation in $\theta(\xi)$ *via* M.

Figure 10: Fluctuation in $\theta(\xi)$ *via* Rd.

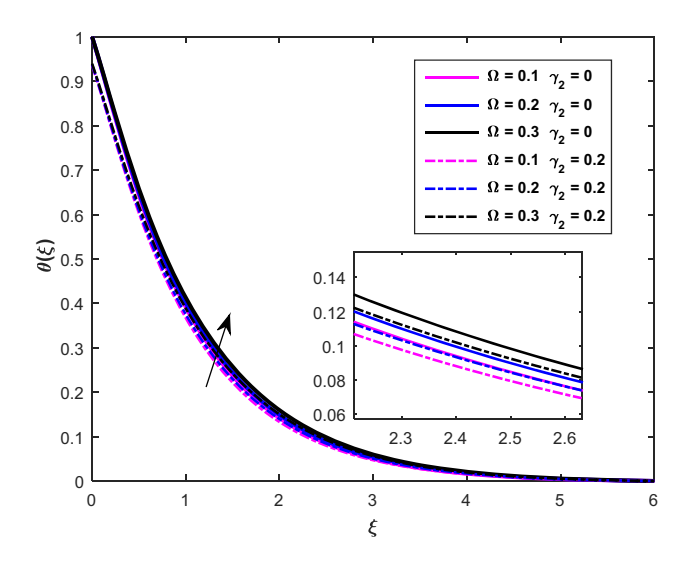


Figure 11: Fluctuation in $\theta(\xi)$ *via* Ω .

thermophysical features of pure fluid and nanoparticles. Table 2 shows the comparison of f''(0) with the varying values of Ω . The results are closely matched with the published work [48,52,53].

Table 3 illustrates the impact of (M) and (K_p) on the skin friction coefficient under slip ($y_1 = 0.2$) and no-slip $(y_1 = 0)$ conditions. Analysis of Table 3 reveals that for the no-slip condition ($y_1 = 0$), the skin friction coefficient increases with escalation in M and K_p . Similarly, for the slip condition ($\gamma_1 = 0.2$), the skin friction coefficient of the hybrid nanofluid also experiences an increase with elevated values of $K_{\rm p}$ and M. This indicates that higher estimates of $K_{\rm p}$ and M contribute to an enhanced skin friction coefficient. In the absence of slip $(y_1 = 0)$, fluid flow encounters significant resistance. For escalation in velocity slip factor the flow resistance diminishes leading to a reduction in skin friction. Table 4 represents the result of the hybrid nanofluid Nusselt number under thermal slip ($\gamma_2 = 0.2$) and no-slip ($\gamma_2 = 0$) conditions, considering varying values of (Ec), magnetic field, heat source and radiation factors. The findings in Table 4 demonstrate that for the thermal slip ($y_2 = 0.2$) and no-slip

Table 3: Influence of K_p and M on f''(0) when $\gamma_1 = 0$ and $\gamma_1 = 0.2$

$\overline{K_{\mathrm{p}}}$	М	$y_1 = 0$	$y_1 = 0.2$	
		<i>f</i> "(0)	f"(0)	
0.1	0.4	0.7687	0.3958	
0.2		0.8912	0.4341	
0.3		0.9992	0.4635	
0.1	1.0	0.9616	0.4536	
	2.0	1.0734	0.4816	
	3.0	1.1759	0.5045	

 $(y_2 = 0)$ conditions, Nusselt number increases with escalation in Rd. Additionally, Table 4 examines the reduction in Nusselt number for M, Ec, and Q_t under thermal slip ($\gamma_2 = 0.2$) and no-slip ($y_2 = 0$) conditions. Figure 1 shows the flow geometry. The effect of different physical parameters on velocities (primary $f'(\xi)$ and secondary $g(\xi)$) and temperature are shown in Figures 2–11. The impact of M on $f'(\xi)$ and $g(\xi)$ with $y_1 = 0$ and $y_1 = 0.2$ are portrayed in Figures 2 and 3. It illustrates that when M improved the curves $f'(\xi)$ dropped. The augmentation of M amplifies the Lorentz force which performs in the opposite direction to fluid flow and induces current within the fluid layers leading to an increase in the resistive force between pure fluid and nanoparticles. This in turn causes a reduction in $f'(\xi)$ field. It is noteworthy that the decline in $f'(\xi)$ is more pronounced under the $(\gamma_1 = 0)$ condition. When $(y_1 = 0.2)$ condition prevails the resistance to fluid flow is notably high. While direct impact is seen for heightened vales of M on $g(\xi)$. The velocity in the secondary direction $g(\xi)$ escalates with M. Table 3 illustrates that raising the magnetic numbers the skin friction enhanced for the no slip $(y_1 = 0)$ condition as compared to the slip $(\gamma_1 = 0.2)$ condition. The porosity parameter denoted by K_p serves as a dimensionless quantity that characterizes the extent of porosity in a fluid. In Figure 4, the $f'(\xi)$ profile is depicted for various values of the K_p . This shows a reduction in $f'(\xi)$ with the growing values in K_p when $\gamma_1 = 0$ and $y_1 = 0.2$. As the permeability parameter enhances there is an associated rise in resistance to fluid motion, leading to a decrease in $f'(\xi)$. This phenomenon occurs because escalation in K_p heightens the porous layer more for $\gamma_1 = 0$ than $y_1 = 0.2$ and also reduces the width of the momentum layer at boundary. Figures 5 and 6 illustrate the impact of Ω in the presence and absence of velocity slip parameters on $f'(\xi)$ and $g'(\xi)$. These figures demonstrate that an escalation in

Table 4: Influence of Ec and M on Nu_n when $y_2 = 0$ and $y_2 = 0.2$

Ec	M	Rd	Q _t	$y_2 = 0$ Nu_n	$y_2 = 0.2$ Nu_n
0.1	0.4	0.1	0.1	1.0405	0.8979
0.3				0.7213	0.6224
0.5				0.4021	0.3469
0.1	0.5			0.8976	0.7853
	0.6			0.8640	0.7584
	0.7			0.8314	0.7322
	0.4	0.3		1.4272	1.2042
		0.5		1.8631	1.5394
		0.7		2.3438	1.8990
		0.1	0.2	1.0405	0.8979
			0.3	0.7641	0.6806
			0.4	0.2156	0.2052

the magnitude of Ω causes retardation in $f'(\xi)$ and $g(\xi)$. In a physical point of view when the fluid rotates centrifugal force acts outward, which opposes the inward flow creating resistance. This resistance declines $f'(\xi)$ and $g(\xi)$. Furthermore enhanced Ω , augments the viscous effects in the boundary layer. This additional force escalates the friction on the fluid which dissipates kinetic energy and decelerates $f'(\xi)$ and $g'(\xi)$. As a result, elevated Ω values introduce additional resistance to the fluid, causing the velocity components to exhibit a decreasing trend with Ω . Under thermal slip ($\gamma_2 = 0.2$) and no-slip ($\gamma_2 = 0$) conditions, Figure 7 elucidates how the hybrid nanofluid temperature $\theta(\xi)$ responds to the variation in M. Notably, an augmentation in fluid temperature $\theta(\xi)$ is observed as M fluctuates. The deceleration of fluid motion evident from the velocity profile is a consequence of the heightened M. This diminished fluid motion facilitates the exchange of kinetic energy into heat energy contributing to enrich $\theta(\xi)$. Additionally, the thermal and momentum layers at the boundary become thinner with an increased M. This thinning is associated with an inverse relationship between the density of fluid and M. Consequently, elevation M leads to a reduction fluid density and growing $\theta(\xi)$. Figure 8 examines the impact of the Ec on $\theta(\xi)$ under thermal slip ($\gamma_2 = 0.2$) and no-slip ($\gamma_2 = 0$) conditions, It is observed that an increase in Ec enhances the temperature of the hybrid nanofluid. This phenomenon can be attributed to the accelerated conversion of mechanical energy into thermal energy, facilitated by the higher Ec, resulting in an overall rise in fluid temperature $\theta(\xi)$. Physically, Ec has a relationship between the flow of kinetic energy and heat enthalpy variation. With an increase in Ec, kinetic energy of hybrid nanofluid amplified. Moreover, temperature is commonly defined as the kinetic energy; therefore, the higher values of Ec amplified the $\theta(\xi)$ of hybrid nanofluid. From the figure, it is also clear that for no slip condition, the temperature is escalated more than slip effect. The reason is that when the thermal slip is present then less heat is transferred from the surface to the liquid. Figure 9 examines the impact of varying values of Q_t on $\theta(\xi)$ under thermal slip $(\gamma_2 = 0.2)$ and no-slip $(\gamma_2 = 0)$ conditions. This figure illustrates that as Q_t upsurges, the temperature profile $\theta(\xi)$ for the slip conditions ($\gamma_2 = 0.2$) experiences more amplification than the no-slip condition ($\gamma_2 = 0$). Q > 0 serve as heat generators, leading to substantial thermal energy release from the boundary layer into the flow. This process significantly enhances the energy field. For both cases, $\theta(\xi)$ graph grows with a higher estimation of Q_t . The effect of Rd on $\theta(\xi)$ in the presence of thermal slip ($\gamma_2 = 0.2$) and no-slip ($\gamma_2 = 0$) scenario is illustrated in Figure 10. Figure 10 shows that as Rd gets larger, then $\theta(\xi)$ profile gets decline. Figure 11 illustrates the impact of Ω on $\theta(\xi)$. An elevation in Ω corresponds to an increase in $\theta(\xi)$. This implies that higher values of Ω lead to a thicker thermal boundary layer. The stretching surface responds to the augmented Ω by rotating at a faster pace, resulting in heightened

centrifugal forces acting on the hybrid nanofluid. This increase in centrifugal forces plays a role in converting kinetic energy into thermal energy, consequently raising the temperature. The heating observed may be attributed to the influence of centrifugal force.

7 Conclusion

This article aims to explore the three-dimensional MHD hybrid nanofluid flow across an enlarging porous surface. The investigation incorporates the influences of thermal radiation magnetic field, heat generation viscous dissipation, and joule heating. The chosen scenario involves a hybrid nanofluid flow within a rotating frame accounting for both velocity and thermal slip conditions. The model developed for this study encompasses momentum and energy equations. The key findings of the present study are as follows:

- · The skin friction coefficient of the hybrid nanofluid is enhanced with a higher number of magnetic and porosity parameters under slip and no-slip conditions.
- The rotation parameter contributes to elevated surface friction resulting in a decrease in both primary and secondary velocities while amplifying the temperature profile.
- Augmentation of the Eckert number, heat generation parameter, and rotation parameters enhance the temperature profile under both slip and no-slip conditions.
- · Under both slip and no-slip conditions, an elevation in the magnetic field parameter is associated with a decrease in primary velocity while simultaneously improving the secondary velocity.
- The primary velocity shows a decreasing trend with the escalating porosity parameter in the presence of slip and no-slip effects.
- The Nusselt number is amplified with radiation parameter while the opposite effect is observed for magnetic and Eckert number and heat source parameter for both thermal slip and no-slip conditions.

Acknowledgments: The authors acknowledge the reviewers for their constructive comments. This work was supported by the Deanship of Scientific Research, Vice Presidency for Graduate Studies and Scientific Research, King Faisal University, Saudi Arabia (KFU241357).

Funding information: This work was supported by the Deanship of Scientific Research, Vice Presidency for Graduate Studies and Scientific Research, King Faisal University, Saudi Arabia (KFU241357).

Author contributions: All authors have accepted responsibility for the entire content of this manuscript and approved its submission.

Conflict of interest: The authors state no conflict of interest.

Data availability statement: All data generated or analysed during this study are included in this published article.

References

- [1] Choi, S. U. S. Enhancing thermal conductivity of fluids with nanoparticles. American Society of Mechanical Engineers, Fluids Engineering Division FED, Vol. 231, 1995, pp. 99–105.
- [2] Aguilar, T., I. Carrillo-Berdugo, P. Martínez-Merino, A. Yasinskiy, M. Rodríguez-Fernández, and J. Navas. Improving stability and thermal properties of TiO 2-based nanofluids for concentrating solar energy using two methods of preparation. *Journal of Thermal Analysis and Calorimetry*, Vol. 144, 2021, pp. 895–905.
- [3] Mehta, B., D. Subhedar, H. Panchal, and Z. Said. Synthesis, stability, thermophysical properties and heat transfer applications of nanofluid–A review. *Journal of Molecular Liquids*, Vol. 364, 2022, id. 120034.
- [4] Kalsi, S., S. Kumar, A. Kumar, T. Alam, and D. Dobrotă. Thermophysical properties of nanofluids and their potential applications in heat transfer enhancement: A review. *Arabian Journal of Chemistry*, 2023, id. 105272.
- [5] Ajeeb, W., R. R. S. T. da Silva, and S. M. S. Murshed. Experimental investigation of heat transfer performance of Al2O3 nanofluids in a compact plate heat exchanger. *Applied Thermal Engineering*, Vol. 218, 2023, id. 119321.
- [6] Khan, A., M. A. Alyami, W. Alghamdi, M. M. Alqarni, M. F. Yassen, and E. Tag Eldin. Thermal examination for the micropolar gold-blood nanofluid flow through a permeable channel subject to gyrotactic microorganisms. Frontiers in Energy Research, Vol. 10, 2022, id. 993247.
- [7] Algehyne, E. A., F. M. Alamrani, A. Khan, K. A. Khan, S. A. Lone, and A. Saeed. On thermal distribution of MHD mixed convective flow of a Casson hybrid nanofluid over an exponentially stretching surface with impact of chemical reaction and ohmic heating. *Colloid and Polymer Science*, Vol. 302, 2024, pp. 503–516.
- [8] Chu, Y., S. Bashir, M. Ramzan, and M. Y. Malik. Model-based comparative study of magnetohydrodynamics unsteady hybrid nanofluid flow between two infinite parallel plates with particle shape effects. *Mathematical Methods in the Applied Sciences*, Vol. 46, 2023, pp. 11568–11582.
- [9] Eid, M. R. and M. A. Nafe. Thermal conductivity variation and heat generation effects on magneto-hybrid nanofluid flow in a porous medium with slip condition. *Waves in Random and Complex Media*, 32, 2022, pp. 1103–1127.
- [10] Ali, B., S. Jubair, A. Aluraikan, M. Abd El-Rahman, S. M. Eldin, and H. A. E.-W. Khalifa. Numerical investigation of heat source induced thermal slip effect on trihybrid nanofluid flow over a stretching surface. *Results in Engineering*, Vol. 20, 2023, id. 101536.
- [11] Nagaraja, K. V., U. Khan, J. K. Madhukesh, A. M. Hassan, B. C. Prasannakumara, N. Ben Kahla, et al. Heat and mass transfer

- analysis of assisting and opposing radiative flow conveying ternary hybrid nanofluid over an exponentially stretching surface. *Scientific Reports*, Vol. 13, 2023, id. 14795.
- [12] Darvesh, A., G. C. Altamirano, M. Sánchez-Chero, W. R. M. Zamora, F. G. Campos, T. Sajid, et al. Variable chemical process and radiative nonlinear impact on magnetohydrodynamics Cross nanofluid: An approach toward controlling global warming. *Heat Transfer*, Vol. 52, 2023, pp. 2559–2575.
- [13] Tag El Din, E. S. M., T. Sajid, W. Jamshed, S. Z. H. Shah, M. R. Eid, A. Ayub, et al. Cross electromagnetic nanofluid flow examination with infinite shear rate viscosity and melting heat through Skan-Falkner wedge. *Open Physics*, Vol. 20, 2022, pp. 1233–1249.
- [14] El Din, S. M., A. Darvesh, A. Ayub, T. Sajid, W. Jamshed, M. R. Eid, et al. Quadratic multiple regression model and spectral relaxation approach for carreau nanofluid inclined magnetized dipole along stagnation point geometry. *Scientific Reports*, Vol. 12, 2022, id. 17337.
- [15] Bejawada, S. G. and M. M. Nandeppanavar. Effect of thermal radiation on magnetohydrodynamics heat transfer micropolar fluid flow over a vertical moving porous plate. *Experimental and Computational Multiphase Flow*, Vol. 5, 2023, pp. 149–158.
- [16] Roy, K., P. Devi, and P. Kumar. Magnetic-field induced sustainable electrochemical energy harvesting and storage devices: Recent progress, opportunities, and future perspectives. *Nano Energy*, Vol. 87, 2021, id. 106119.
- [17] Raje, A., F. Koyani, A. A. Bhise, and K. Ramesh. Heat transfer and entropy optimization for unsteady MHD Casson fluid flow through a porous cylinder: Applications in nuclear reactors. *International Journal of Modern Physics B: Condensed Matter Physics, Statistical Physics, Applied Physics*, Vol. 37, 2023, id. 2350293.
- [18] Safdar, M., M. Ijaz Khan, R. A. Khan, S. Taj, F. Abbas, S. Elattar, et al. Analytic solutions for the MHD flow and heat transfer in a thin liquid film over an unsteady stretching surface with Lie symmetry and homotopy analysis method. Waves in Random and Complex Media, 33, 2023, pp. 442–460.
- [19] Rasool, G., N. A. Ahammad, M. R. Ali, N. A. Shah, X. Wang, A. Shafiq, et al. Hydrothermal and mass aspects of MHD non-Darcian convective flows of radiating thixotropic nanofluids nearby a horizontal stretchable surface: passive control strategy. *Case Studies in Thermal Engineering*, Vol. 42, 2023, id. 102654.
- [20] Obalalu, A. M., T. Oreyeni, A. Abbas, M. A. Memon, U. Khan, E.-S. M. Sherif, et al. Implication of electromagnetohydrodynamic and heat transfer analysis in nanomaterial flow over a stretched surface: Applications in solar energy. *Case Studies in Thermal Engineering*, Vol. 49, 2023, id. 103381.
- [21] Dharmaiah, G., J. L. R. Prasad, K. S. Balamurugan, I. Nurhidayat, U. Fernandez-Gamiz, and S. Noeiaghdam. Performance of magnetic dipole contribution on ferromagnetic non-Newtonian radiative MHD blood flow: An application of biotechnology and medical sciences. *Heliyon*, Vol. 9, 2023.
- [22] Ayub, A., T. Sajid, W. Jamshed, W. R. M. Zamora, L. A. V. More, L. M. G. Talledo, et al. Activation energy and inclination magnetic dipole influences on Carreau nanofluid flowing via cylindrical channel with an infinite shearing rate. *Applied Sciences*, Vol. 12, 2022, id. 8779.
- [23] Wang, F., A. M. Saeed, V. Puneeth, N. A. Shah, M. S. Anwar, K. Geudri, et al. Heat and mass transfer of Ag-H2O nano-thin film flowing over a porous medium: A modified Buongiorno's model. *Chinese Journal of Physics*, Vol. 84, 2023, pp. 330–342.
- [24] Alsulami, M. D., R. Naveen Kumar, R. J. Punith Gowda, and B. C. Prasannakumara. Analysis of heat transfer using Local thermal non-equilibrium conditions for a non-Newtonian fluid flow containing

- Ti6Al4V and AA7075 nanoparticles in a porous media. ZAMM-Journal of Applied Mathematics and Mechanics/Zeitschrift für Angewandte Mathematik und Mechanik, Vol. 103, 2023, id. e202100360.
- [25] Herrera-Hernandez, E. C., C. G. Aguilar-Madera, G. Espinosa-Paredes, and D. Hernandez. Modeling single-phase fluid flow in porous media through non-local fractal continuum equation. Journal of Engineering Mathematics, Vol. 138, 2023, id. 8.
- [26] Zahor, F. A., R. Jain, A. O. Ali, and V. G. Masanja. Modeling entropy generation of magnetohydrodynamics flow of nanofluid in a porous medium: A review. International Journal of Numerical Methods for Heat & Fluid Flow, Vol. 33, 2023, pp. 751-771.
- [27] Khan, A., Z. Iqbal, N. A. Ahammad, M. O. Sidi, S. Elattar, S. Awad, et al. Bioconvection Maxwell nanofluid flow over a stretching cylinder influenced by chemically reactive activation energy surrounded by a permeable medium. Frontiers of Physics, Vol. 10, 2023, id. 1348.
- [28] Darvesh, A., T. Sajid, W. Jamshed, A. Ayub, S. Z. H. Shah, M. R. Eid, et al. Rheology of variable viscosity-based mixed convective inclined magnetized cross nanofluid with varying thermal conductivity. Applied Sciences, Vol. 12, 2022, id. 9041.
- [29] Rakpakdee, W., M. Motozawa, M. Fukuta, and W. Chaiworapuek. Characteristics of heat transfer and flow resistance of magnetic fluid flow through porous media combined with magnetic field effect. Experimental Thermal and Fluid Science, Vol. 144, 2023, id. 110851.
- Ayub, A., S. Z. H. Shah, Z. Sabir, N. S. Rao, R. Sadat, and M. R. Ali. Spectral relaxation approach and velocity slip stagnation point flow of inclined magnetized cross-nanofluid with a quadratic multiple regression model. Waves in Random and Complex Media, 2022, pp. 1–25.
- [31] Rasheed, H. U., S. Islam, Zeeshan, T. Abbas, and J. Khan. Analytical treatment of MHD flow and chemically reactive Casson fluid with Joule heating and variable viscosity effect. Waves in Random and Complex Media, 2022, pp. 1-17.
- [32] Irfan, M., M. S. Anwar, I. Kebail, and W. A. Khan. Thermal study on the performance of Joule heating and Sour-Dufour influence on nonlinear mixed convection radiative flow of Carreau nanofluid. Tribology International, Vol. 188, 2023, id. 108789.
- [33] Liao, X., Y. J. Lim, M. Khayet, Y. Liao, L. Yao, Y. Zhao, et al. Applications of electrically conductive membranes in water treatment via membrane distillation: Joule heating, membrane fouling/scaling/wetting mitigation and monitoring. Water Research, 2023, id. 120511.
- [34] Wang, Y., L. Ren, Z. Yang, S. Shen, Z. Deng, Q. Yuan, et al. Heat management technology for solid-state high voltage and high repetitive pulse generators: Towards better effects and reliability. High Voltage, Vol. 9, 2024, pp. 2-21.
- [35] Idris, S., A. Jamaludin, R. Nazar, and I. Pop. Radiative MHD flow of hybrid nanofluid over permeable moving plate with Joule heating and thermal slip effects. Alexandria Engineering Journal, Vol. 83, 2023, pp. 222-233.
- [36] Khan, A., Z. Shah, E. Alzahrani, and S. Islam. Entropy generation and thermal analysis for rotary motion of hydromagnetic Casson nanofluid past a rotating cylinder with Joule heating effect. International Communications in Heat and Mass Transfer, Vol. 119, 2020, id. 104979.
- [37] Ravikumar, S., M. Rafiq, D. Abduvalieva, and F. A. Awwad. Effects of Joule heating and reaction mechanisms on couple stress fluid flow with peristalsis in the presence of a porous material through an inclined channel. Open Physics, Vol. 21, 2023, id. 20230118.
- [38] Rilwan, U. S., M. O. Oni, B. K. Jha, and H. M. Jibril. Analysis of Joule heating and viscous dissipation on electromagnetohydrodynamic flow with electroosmotic effect in a porous microchannel: A heat transfer miniature enhancement. Heat Transfer, 2023.

- [39] Tanveer, A. and M. B. Ashraf. Mixed convective flow of Sisko nanofluids over a curved surface with entropy generation and Joule heating. Arabian Journal for Science and Engineering, Vol. 48, 2023, pp. 11263-11275.
- [40] Chaplina, T. Transfer of substance in vortex and wave flows in one-component and multi-component environment, Springer Nature, Switzerland, 2023.
- Balasundaram, H., S. Sathyamoorthi, U. Fernandez-Gamiz, S. Noeiaghdam, and S. S. Santra. Hydrocephalic cerebrospinal fluid flowing rotationally with pulsatile boundaries: A mathematical simulation of the thermodynamical approach. Theoretical and Applied Mechanics Letters, Vol. 13, 2023, id. 100418.
- [42] Che, J., R. You, W. Chen, and H. Li. Investigation on the compressibility characteristics of low mach number laminar flow in rotating channel. ArXiv Prepr. ArXiv2308.08225, 2023.
- [43] Basriati, S. and H. Saleh. Mathematical modeling of unsteady convective flow analysis of water and nano-encapsulated phase change particles in composite enclosure subject to rotation. Journal of Energy Storage, Vol. 72, 2023, id. 108393.
- [44] Khan, A., A. Saeed, T. Gul, S. Mukhtar, I. Ali, and M. Jawad. Radiative swirl motion of hydromagnetic Casson nanofluid flow over rotary cylinder using Joule dissipation impact. Physica Scripta, Vol. 96, 2021, id. 45206.
- [45] Acharya, N. and K. Das. Three-dimensional rotating flow of Cu-Al2O3/kerosene oil hybrid nanofluid in presence of activation energy and thermal radiation. Numerical Heat Transfer, Part A: Applications, Vol. 84, 2023, pp. 586-603.
- Kumar, A., A. P. Dash, A. K. Ray, P. Sethy, and I. Kasireddy. Unsteady mixed convective flow of hybrid nanofluid past a rotating sphere with heat generation/absorption: an impact of shape factor. International Journal of Numerical Methods for Heat & Fluid Flow, Vol. 33, 2023, pp. 3691-3715.
- [47] Shoaib, M., M. A. Z. Raja, M. T. Sabir, S. Islam, Z. Shah, P. Kumam, et al. Numerical investigation for rotating flow of MHD hybrid nanofluid with thermal radiation over a stretching sheet. Scientific Reports, Vol. 10, 2020, pp. 1-15.
- Dawar, A., T. Thumma, S. Islam, and Z. Shah. Optimization of response function on hydromagnetic buoyancy-driven rotating flow considering particle diameter and interfacial layer effects: Homotopy and sensitivity analysis. International Communications in Heat and Mass Transfer, Vol. 144, 2023, id. 106770.
- Kho, Y. B., A. Hussanan, M. K. A. Mohamed, and M. Z. Salleh. Heat and mass transfer analysis on flow of Williamson nanofluid with thermal and velocity slips: Buongiorno model. Propulsion and Power Research, Vol. 8, 2019, pp. 243-252.
- Mahanthesh, B., B. J. Gireesha, and R. S. R. Gorla. Heat and mass transfer effects on the mixed convective flow of chemically reacting nanofluid past a moving/stationary vertical plate. Alexandria Engineering Journal, Vol. 55, 2016, pp. 569-581.
- Khashi'ie, N. S., N. M. Arifin, I. Pop, and N. S. Wahid. Flow and heat [51] transfer of hybrid nanofluid over a permeable shrinking cylinder with Joule heating: A comparative analysis. Alexandria Engineering Journal, Vol. 59, 2020, pp. 1787-1798.
- [52] Hussain, A., M. A. Elkotb, M. Arshad, A. Rehman, K. Sooppy Nisar, A. Hassan, et al. Computational investigation of the combined impact of nonlinear radiation and magnetic field on three-dimensional rotational nanofluid flow across a stretchy surface. Processes, Vol. 9, 2021, id. 1453.
- Nazir, U., M. Sohail, M. B. Hafeez, and M. Krawczuk. Significant production of thermal energy in partially ionized hyperbolic tangent material based on ternary hybrid nanomaterials. Energies, Vol. 14, 2021, id. 6911.